

# Image Generation Via Minimizing Fréchet Distance in Discriminator Feature Space\*

Khoa D. Doan<sup>1</sup> Saurav Manchanda<sup>2</sup> Fengjiao Wang<sup>3</sup>, Sathya Keerthi<sup>4</sup>,  
Avradeep Bhowmik<sup>3</sup>, and Chandan K. Reddy<sup>1</sup>

<sup>1</sup> Virginia Tech, Arlington, USA  
khoadoan@vt.edu, reddy@cs.vt.edu

<sup>2</sup> University of Minnesota, USA  
manch043@umn.edu

<sup>3</sup> Amazon, USA

w.fengjiao@gmail.com, avradeep.1@gmail.com

<sup>4</sup> LinkedIn Corporation, USA  
keselvaraj@linkedin.com

**Abstract.** For a given image generation problem, the intrinsic image manifold is often low dimensional. We use the intuition that it is much better to train the GAN generator by minimizing the distributional distance between real and generated images in a small dimensional feature space representing such a manifold than on the original pixel-space. We use the feature space of the GAN discriminator for such a representation. For distributional distance, we employ one of two choices: the Fréchet distance or direct optimal transport (OT); these respectively lead us to two new GAN methods: Fréchet-GAN and OT-GAN. The idea of employing Fréchet distance comes from the success of Fréchet Inception Distance as a solid evaluation metric in image generation. Fréchet-GAN is attractive in several ways. We propose an efficient, numerically stable approach to calculate the Fréchet distance and its gradient. The Fréchet distance estimation requires a significantly less computation time than OT; this allows Fréchet-GAN to use much larger mini-batch size in training than OT. More importantly, we conduct experiments on a number of benchmark datasets and show that Fréchet-GAN (in particular) and OT-GAN have significantly better image generation capabilities than the existing representative primal and dual GAN approaches based on the Wasserstein distance.

## 1 Introduction

There has been a great amount of interest in generative modeling in recent years. This is driven largely by recently proposed generative models such as Generative Adversarial Networks (GANs) and Variational Autoencoders (VAEs). Different from classical generative models which directly sample from the high-dimensional space [3,24], GANs and VAEs sample from a low-dimensional space and rely on

---

\* This work was done when several of the authors were in Criteo Inc., Palo Alto, USA.

deep neural networks to transform these samples into the high-dimensional target space. While VAEs have an appealing probabilistic interpretation, in the image domain their generated samples are often overly smooth. GANs are known to generate more realistic visual images, but training them has several challenges, most notably mode collapse and vanishing gradient.

The original GAN, proposed by [11], suffers from both frequent mode collapse and vanishing gradient. To address such problems, [1,21] proposes to replace the Jensen-Shannon divergence objective in the original GAN with the Wasserstein distance objective. Wasserstein distance has a weaker topology assumption; thus the generated distribution more easily converges to the true distribution than in the case of some other divergences, without the mode collapse and gradient saturation problems in training. However, estimating the Wasserstein distance is a nontrivial task. Generally, there exist two main classes of approaches: 1) from the dual domain and 2) from the primal domain.

Because of the intractability of estimating the Wasserstein distance from the primal domain, [21] proposes to estimate the Wasserstein distance by employing Kantorovich-Rubinstein duality and parameterizes the space of all 1-Lipschitz functions by a fixed network (critic), whose parameters are clamped to ensure the required Lipschitz smoothness. Later, WGAN-GP [12] and WGAN-SN [23] constrains the Lipschitz smoothness by using gradient-clipping regularization and gradient normalization, respectively. However, these approaches can have a significant approximation error when the learnable function space, which is controlled by their hyperparameters, is too large or too small. Furthermore, the dual domain requires the minimax setup, which is generally hard to optimize with problems such saddle-point.

Alternatively, from the primal domain, [15] estimates the empirical Wasserstein distance directly from the samples by solving the Optimal Transport (OT) problem. While solving the OT problem is a valid and promising direction, the computational cost, which is  $O(N^{2.5} \log N)$  where  $N$  is the number of samples, is expensive. The empirical Wasserstein distance is also known to have high-variance and exponential sample complexity [8,7,10]. Furthermore, minimizing the OT cost on the pixel space does not work for high-dimensional images [15].

To address the exponential sample-complexity problem, Sliced Wasserstein GAN (SWG) [8] proposes to estimate the Sliced-Wasserstein distance, which randomly projects the data into many one-dimensional directions and approximates the Sliced-Wasserstein distance by averaging the one-dimensional Wasserstein distances along these directions. SWG has a polynomial sample-complexity [8]. However, Sliced-Wasserstein distance is a very different metric, thus it does not have all the nice geometrical properties of Wasserstein distance [10]. Furthermore, in the high-dimensional space, a random one-dimensional direction will not likely lie on the data manifold, thus its Wasserstein distance is likely to be close to zero. For such a reason, SWG requires a large-number of random projections, which defeats its computational advantage as compared to OT. Later, to address this problem of SWG, Max-Sliced Wasserstein GAN (Max-SWG) proposes to find the best direction and minimize the distance along this direction [7]. Max-SWG

shows a significant improvement over SWG while having a lower computational cost and memory footprint, and it is an important baseline to compare against.

Our work started as an effort to improve the primal Wasserstein distance approach. Working on the raw, high dimensional image pixel space is clearly inappropriate. Most image generation problems have an intrinsic image manifold that is low dimensional and so it is better to work with a suitable low dimensional feature space that is problem/dataset specific. The main novelty of this paper comes from the use of the feature space of the GAN discriminator (that is designed to distinguish real and generated images) for this purpose.

Having settled the feature space to work with, we also explore the type of distributional distance to employ. We could simply use the Wasserstein distance computed by OT. This leads us to our OT-GAN method. Alternatively, motivated by the success of Fréchet Inception Distance as a solid evaluation metric in image generation problems, we also try the Fréchet distance in the discriminator feature space. We call the resulting method as Fréchet-GAN. We develop all the algorithmic and design details associated with Fréchet-GAN and demonstrate that it is attractive in several ways, including a strong performance on several image generation benchmarks.

The main contributions of our paper can be summarized as follows.

- We propose Fréchet-GAN and OT-GAN as novel and highly performing alternatives for existing GAN methods.
- We develop all the algorithmic and design details needed for their efficient implementation, e.g., the computation of the distances and their gradients.
- We demonstrate the superiority of the proposed models, especially of Fréchet-GAN, over other representative GAN approaches. Specifically, Fréchet-GAN achieves a significant improvement in terms of both, the quality of the generated images and the Fréchet Inception Distance metric, on the popular MNIST, CIFAR-10, CELEB-A and LSUN-Bedroom benchmark datasets.

The paper is organized as follows. In Section 2, we provide a review of the related primal GANs to our proposed models, noting the importance of minimizing the distributional distance in the low-dimensional feature space. In Section 3, we describe the details of our proposed methods. Then, we present the quantitative and qualitative experimental results in Section 4. Finally, Section 5 gives the conclusion.

## 2 Background

We begin by summarizing two related approaches of estimating the Wasserstein distance from the primal domain. Then, we discuss the importance of moving away from the pixel-space to a more suitable, low-dimensional feature space where the distributional distance is optimized. Finally, we discuss the Fréchet Inception Distance, which is the motivation behind our Fréchet-GAN model.

## 2.1 Primal Wasserstein Distances

In generative modeling, we learn to estimate the density  $\mathbb{P}_d$  only from its empirical samples  $\mathcal{D} = \{x|x \sim \mathbb{P}_d\}$ . Different from the explicit generative models [24,3], GANs model  $\mathbb{P}_d$  as  $\mathbb{P}_g$  implicitly through a mapping function from a low-dimensional latent space  $\mathbb{P}_z$ . Most GANs can be viewed as minimizing the distance between  $\mathbb{P}_d$  and  $\mathbb{P}_g$ . One interesting distance of measures is the Wasserstein distance. Wasserstein distance has a weaker topology assumption and is the de facto metric for comparing distributions with non-overlapping supports. Minimizing the Wasserstein distance allows the generated distribution to more easily converge to the true distribution than in the case of other divergences, such as Jensen-Shannon divergence. Given the  $L^p$  distance function  $d(x, y)$ , the Wasserstein-p distance between two distributions  $\mathbb{P}_d$  and  $\mathbb{P}_g$  is defined as follows:

$$W_p(\mathbb{P}_d, \mathbb{P}_g) = \inf_{\gamma \in \Pi(\mathbb{P}_d, \mathbb{P}_g)} \int_{(x,y) \sim \gamma} p(x, y) d^p(x, y) dx dy \quad (1)$$

where  $\Pi(\mathbb{P}_d, \mathbb{P}_g)$  is the set of all joint distributions of  $x$  and  $y$  whose marginals are  $\mathbb{P}_d$  and  $\mathbb{P}_g$ , respectively.

Because directly estimating the Wasserstein distance is highly intractable, [21] employs Kantorovich-Rubinstein duality to estimate the Wasserstein-1 distance as follows:

$$W_1(\mathbb{P}_d, \mathbb{P}_g) = \sup_{\|f\|_L \leq 1} E_{x \sim \mathbb{P}_g}[f(x)] - E_{x \sim \mathbb{P}_d}[f(x)] \quad (2)$$

where  $f$  is a 1-Lipschitz continuous function. In practice, the function  $f$  can be represented by a neural network. Enforcing the Lipschitz smoothness is still an open problem. Popular strategies such as weight clamping, gradient clipping and gradient normalization are employed [21,12,23]. However, these techniques suffer from the Lipschitz-smoothness approximation in the parameterized function space. Consequently, training these models remain inefficient in practice because of their additional hyperparameter tuning.

Recently, [15] proposes to directly estimate the Wasserstein-p distance from its primal domain by solving the OT problem from the empirical samples. Let  $\mathcal{D}$  and  $\mathcal{F}$  be the empirical samples which are drawn from  $\mathbb{P}_d$  and  $\mathbb{P}_g$  respective. Given a sample  $x_i$  from  $\mathcal{D}$  and a sample  $y_j$  from  $\mathcal{F}$ , the  $L^p$  distance function is parameterized by the generator's parameters  $\Theta_G$  and denoted as  $d_{\Theta_G}(x_i, y_j)$ . The OT cost between  $\mathcal{D}$  and  $\mathcal{F}$ , is calculated by solving the following linear-sum assignment problem:

$$C(\mathcal{D}, \mathcal{F}) = \min_{\Theta_G} \sum_i^I \sum_j^J m_{i,j} d_{\Theta_G}^p(x_i, y_j) \quad (3)$$

subject to the constraints:

$$\sum_i m_{i,j} = 1 \forall j, \quad \sum_j m_{i,j} = 1 \forall i, \quad m_{i,j} \in \{0, 1\} \forall i, j \quad (4)$$

Note that the matrix  $M$  is a doubly stochastic matrix and the solution is a permutation matrix. Because this method does not have the generator-discriminator

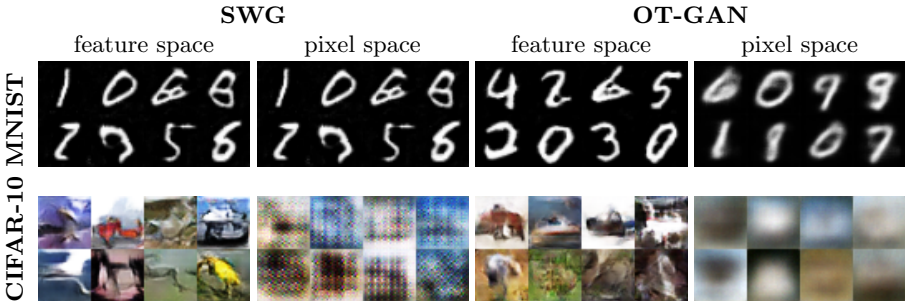


Figure 1: Generated images when minimizing the divergences (Sliced Wasserstein distance and OT) on the pixel versus feature space.

setup, it is no longer a GAN. Clearly, minimizing OT on the high dimensional image pixel space is inappropriate. As shown in Figure 1, the models generate CIFAR-10 images (higher-dimensional) with significant mode collapse or white noise than the generated MNIST images (low-dimensional). Minimizing OT on the original input space only works in domains where the input data is already low-dimensional and the Frobenius distance is suitable [20,9]. Another challenge of using OT is its high computational cost. Solving the linear-sum assignment program has a complexity of  $O(N^{2.5} \log N)$  where  $N$  is the number of samples [5]. Reducing OT’s computational cost is necessary to utilize it in practice [9].

Along the same primal direction, SWG estimates the Sliced Wasserstein distance, which is also a valid distance metric between two distributions [8]. Like OT, in principle, SWG too does not need the generator-discriminator setup. However, as shown in Figure 1, SWG fails to generate meaningful images when it minimizes the Sliced Wasserstein distance in the pixel space. For high-dimensional datasets, SWG transforms the high-dimensional input space into a suitable low-dimensional space. The low-dimensional space is chosen to maximally separates the real and fake samples. Thus, SWG has the generator-discriminator setup, where the discriminator is trained to classify real and fake samples while the generator is trained to minimize the Sliced Wasserstein distance on the projected low-dimensional space. Suppose  $D$  is the discriminator and some intermediate output of  $D$  is defined as  $D'$ . The  $D'(x)$  space is called the **feature space**. SWG learns to generate images by having the following objectives:

$$\min_{\Theta_D} E_{x \sim \mathbb{P}_d}[-\log(D(x))] + E_{x \sim \mathbb{P}_g}[-\log(1 - D(x))] \quad (5)$$

$$\min_{\Theta_G} \frac{1}{|\Omega|} \sum_{\omega \in \Omega} W_2^2(D'(\mathcal{D})\omega, D'(\mathcal{F})\omega) \quad (6)$$

where  $W_2^2$  is the one-dimensional Wasserstein-2 distance in the direction defined by  $\omega$  and  $\Omega$  is the set of one-dimensional random projections. The one-dimensional Wasserstein distance has a trivial computation [8]. While SWG works well in many complex generative modeling tasks, the random projections lose a lot of information even in the feature space  $D'(x)$ . This is because a randomly projected direction is unlikely along the data manifold. Consequently, SWG needs a large

number of random projections to work well, which defeats its computational advantage over OT. Specifically, SWG estimates the Wasserstein distance with a computational cost of  $O(KN \log(N))$ , whose computation complexity is better than the complexity of OT only when  $K$  is smaller than  $N^{1.5}$ . However, in practice, the number of random directions  $K$  is often larger than  $N^{1.5}$ . For example, in [8], for a mini-batch size of 64, SWG needs  $K = 10,000$  projections, which is significantly larger than  $64^{1.5}$ , to generate high-dimensional images. To address this problem, Max-SWG finds the best direction and estimates the Wasserstein distance along this direction [7]. Max-SWG significantly reduces the computational complexity and memory footprint of SWG. Furthermore, Max-SWG can generate images with high visual quality.

## 2.2 Fréchet distance

Given two multivariate Gaussian distributions  $\mathbb{P}_g$  and  $\mathbb{P}_d$  with means  $\mu_g$  and  $\mu_d$  respectively, and covariances  $\Sigma_g$  and  $\Sigma_d$  respectively, the Fréchet distance between  $\mathbb{P}_g$  and  $\mathbb{P}_d$  is defined as follows:

$$\text{FD}(\mathbb{P}_g, \mathbb{P}_d) = \|\mu_d - \mu_g\|^2 + \text{Tr} \left( \Sigma_d + \Sigma_g - 2\sqrt{\Sigma_d \Sigma_g} \right) \quad (7)$$

In the image domain, Fréchet distance is popularly used to calculate the Fréchet Inception Distance (FID) of the generative models. FID is calculated by first extracting the activations of the real and generated images on pool3 layer of the pre-trained InceptionV3 network, then computing the Fréchet distance from the extracted features of the samples [13]. The InceptionV3 network is pre-trained on the ImageNet dataset. Lower FID is generally better and the corresponding generative model is able to generate images with highly realistic visual quality. Interestingly, the Fréchet distance is equivalent to the Wasserstein-2 distance of the two multivariate Gaussian distributions.

## 3 Approach

We consider the problem of improving the existing primal Wasserstein distance approaches in the image generation domain. First, we discuss how to efficiently scale up OT to the high-dimensional image cases using a more suitable, low-dimensional feature space. Then, we propose a novel, computationally efficient alternative to OT. This involves calculating the Fréchet distance between two distributions in the feature space.

### 3.1 Scaling up OT

While minimizing OT in the pixel space is able to generate MNIST digits, the digits are overly smooth (Figure 1), similar to those generated by VAE. We conjecture that this is because of the lack of the discriminator, which discriminates samples as real or fake. Specifically, minimizing the Wasserstein distance in the pixel-space causes the algorithm to easily fall into a local minimum where the

generated distribution  $\mathbb{P}_g$  is the average of other possible distributions that also represent realistic digits. Thus, the discriminator is necessary to penalize the distribution whose digits are visually smooth but unrealistic. Beyond MNIST, OT also fails to generate higher-dimensional images such as CIFAR-10 and CELEB-A. It is known that the Wasserstein distance has an exponential sample complexity [7]: higher-dimensional data need an impractical amount of samples to accurately estimate the Wasserstein distance. While natural images have high dimensions, the intrinsic manifold often lies on a much lower-dimensional subspace. Therefore, directly estimating OT on the pixel-space is highly ineffective. For these reasons, in this paper, we argue that the discriminator is necessary to have OT work effectively on a variety of image datasets.

Inspired by SWG, we employ a discriminator whose primary objective is to find a low-dimensional subspace that best discriminates the real and fake samples. Specifically, suppose that  $D$  is the discriminator function and  $D'$  is the part of  $D$  which we consider as the **feature space**. Instead of minimizing OT between  $\mathbb{P}_g$  and  $\mathbb{P}_d$ , we approximate OT on the output distributions of  $D'$ ; that is, we minimize OT on the distribution of  $D'(\mathcal{D})$ , denoted as  $\mathbb{P}_d^{D'}$ , and the distribution of  $D'(\mathcal{F})$ , denoted as  $\mathbb{P}_g^{D'}$ . In other words, given the generator’s parameters  $\Theta_G$  and the discriminator’s parameters  $\Theta_D$ , we have the following objectives that are independently optimized:

$$\min_{\Theta_D} E_{x \sim \mathbb{P}_d}[-\log(D(x))] + E_{x \sim \mathbb{P}_g}[-\log(1 - D(x))] \quad (8)$$

$$\min_{\Theta_G} C(D'(\mathcal{D}), D'(\mathcal{F})) \quad (9)$$

We call this model OT-GAN. Figure 1 shows the effectiveness of OT-GAN. The generated images, in both MNIST and CIFAR-10 examples, have a significant improvement over the pixel-space minimization. Note that, OT-GAN does not have the minimax setup because the objective functions of the generator and discriminator are different.

### 3.2 GAN based on Fréchet distance

While OT-GAN offers a significant improvement over its pixel-space minimization, the high computational complexity is prohibitive in practice. In this section, we propose a computationally efficient alternative that is based on the Fréchet distance.

Assuming the feature space  $\mathbb{P}_d^{D'}$  and  $\mathbb{P}_g^{D'}$  are multivariate Gaussian distributions, we can approximate the Wasserstein-2 distance via the Fréchet distance, as described in Section 2.2. The means of  $\mathbb{P}_d^{D'}$  and  $\mathbb{P}_g^{D'}$  are  $\mu_d^{D'}$  and  $\mu_g^{D'}$ , respectively, while their covariances are  $\Sigma_d^{D'}$  and  $\Sigma_g^{D'}$ , respectively. Note that only  $\mu_g^{D'}$  and  $\Sigma_g^{D'}$  are functions of the generator’s parameters  $\Theta_G$ . The Fréchet distance of the multivariate Gaussians  $\mathbb{P}_d^{D'}$  and  $\mathbb{P}_g^{D'}$  is defined as:

$$\text{FD}(\mathbb{P}_d^{D'}, \mathbb{P}_g^{D'}) = \|\mu_d^{D'} - \mu_g^{D'}\|^2 + \text{Tr} \left( \Sigma_d^{D'} + \Sigma_g^{D'} - 2\sqrt{\Sigma_d^{D'} \Sigma_g^{D'}} \right) \quad (10)$$

We now describe an efficient algorithm for computing the Fréchet distance. While the Fréchet distance can be analytically calculated, we need to pay special attention to avoid numerical errors, especially when training the model on conventional computing hardware. In Equation 10, computing the values and derivatives (w.r.t  $\Theta_G$ ) of  $\|\mu_d^{D'} - \mu_g^{D'}\|^2$  and  $Tr(\Sigma_g^{D'})$  is trivial. Therefore, we focus the discussion of this section to computing the matrix square root term  $\sqrt{\Sigma_d^{D'} \Sigma_g^{D'}}$  and its derivative  $\partial_{\Theta_G} \sqrt{\Sigma_d^{D'} \Sigma_g^{D'}}$ . Note that  $\Sigma_d^{D'} \Sigma_g^{D'}$  is a  $d \times d$  matrix, where  $d$  is the dimension of the feature space  $D'$ .

In the following discussion, we rely on some useful mathematical results, which will be provided in the Appendix of this paper.

**Computing the matrix square root:** Suppose  $A \in \mathcal{R}^{d \times d}$  is a positive semi-definite (PSD) matrix and its SVD is given by  $S\Sigma S^T$ , where  $\Sigma$  is a diagonal matrix and  $S$  is an orthogonal matrix. Note that the diagonal entries of  $\Sigma$  are non-negative real numbers. Define the matrix  $B$  as follows  $B = S\sqrt{\Sigma}S^T$ .  $B$  is a PSD matrix and  $\sqrt{\Sigma}$  has non-negative diagonal entries. It is trivial to see that  $B$  is the square root matrix of  $A$ . Furthermore, it can be shown that  $B$  is the unique square root of the symmetric, PSD matrix  $A$ .

**Computing the matrix derivative:** Given the PSD matrix  $A \in \mathcal{R}^{d \times d}$  and its square root matrix  $B \in \mathcal{R}^{d \times d}$ , we can derive the following equation by applying implicit differentiation on the equation  $A = BB$ :

$$\partial A = \partial B \times B + B \times \partial B \quad (11)$$

It turns out that this equation has the same form as the Sylvester equation, and there is a closed-form solution for  $\partial B$ , as follows:

$$\text{vec}(\partial B) = (B^T \otimes B)^{-1} \text{vec}(\partial A) \quad (12)$$

where  $\text{vec}(X)$  is a vectorization operation that stacks columns of  $X$  into a column vector, and  $\otimes$  is the Kronecker product. However, this is a naive solution with a high computational cost of  $O(d^3)$ . In practice, we can also employ the Bartels-Stewart algorithm to solve this equation [2]. The Bartels-Stewart algorithm has a computational complexity of  $O(d^{1.5})$ , which is a significant improvement over the naive solution.

In principle, if we can compute  $\sqrt{A}$ , we can compute its derivative,  $\partial\sqrt{A}$ . However, in practice, [16] suggests that the SVD is ill-conditioned when some of the eigenvalues of  $A$  are close to each other. In our experiments, we also observe that the eigenvalues become negative and the gradients become unstable when this condition happens. Therefore, we propose to compute  $\sqrt{A}$  using the Newton-Schultz iterative algorithm [14], which we describe next. The Newton-Schultz algorithm is an extension to the popular Denman-Beaver algorithm [6], but is more efficient because it only involves matrix multiplications instead of calculation of inverses. Let  $A$  be a normalized matrix, and let  $Y_0 = A$  and  $Z_0 = I$ ,

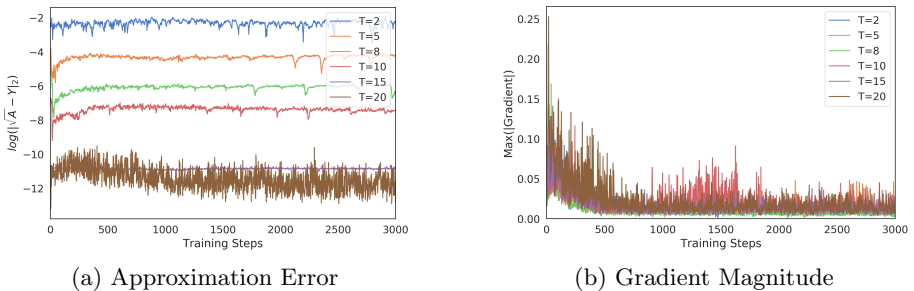


Figure 2: Behavior of our proposed matrix square root calculation during training with different numbers of iterations  $T$ .

where  $I$  is the identity matrix. In each iteration, we update  $Y_{t+1}$  and  $Z_{t+1}$  as:

$$U = \frac{1}{2}(3I - Z_t Y_t), Y_{t+1} = Y_t U, Z = U Z_t \quad (13)$$

When  $t \rightarrow \infty$ , the matrices  $Y$  and  $Z$  converge quadratically to  $A^{1/2}$  and  $A^{-1/2}$ , respectively. Note that, when computing  $\sqrt{A}$  iteratively, we can rely on automatic differentiation, which is supported in most modern deep learning frameworks, to compute its derivative. However, the memory overhead grows linearly with the number of iterations if the computation graph is preserved. Thus, to maintain both numerical accuracy and low-memory overhead, we suggest to first compute  $\sqrt{A}$  iteratively without keeping the computation graph in memory, then solve the Sylvester equation to directly compute its gradient with respect to the parameters. In our experiments, we observe that 10-15 iterations are adequate to converge to a good numerical error in a conventional GPU (Figure 2a). Thus, for simplicity, we rely on the automatic differentiation of the iterative solution to calculate the gradient of  $\sqrt{A}$ . In Figure 2b, we also observe that the gradient of the parameters is stable when we train using this approach.

**Fréchet-GAN** While the pixel distributions  $\mathbb{P}_g$  and especially  $\mathbb{P}_d$  are not multivariate Gaussians, it is possible to enforce the feature space to be multivariate Gaussian, especially when the discriminator is a convolutional neural network. Inspired by the mechanics of calculating FID, we replace the last convolutional layer of  $D'$  by an Average Pooling (AP) layer. Because of the effect of AP and the Central Limit Theorem, the output follows a multivariate Gaussian distribution. Heuristically, we find that using Max Pooling (MP) also yields multivariate Gaussian output in the modified DCGAN architecture [13]. Interestingly, the use of MP yields a significant better result than AP; Although, right now we do not have a precise explanation about this, we conjecture that MP results in a feature space where it is easier for the discriminator to discriminate real and generated examples. Note that the data covariance matrices  $\Sigma_d^{D'}$  and  $\Sigma_g^{D'}$  are PSD.

We call the proposed approach Fréchet-GAN, and the learning algorithm of Fréchet-GAN is summarized in Algorithm 1. The code of Fréchet-GAN is

---

**Algorithm 1:** Fréchet-GAN Training.
 

---

**Input:** The generator’s parameters  $\Theta_G$ , the discriminator’s parameters  $\Theta_D$ , the mini-batch size  $N$ , and the learning rate  $\alpha$ .

```

1 while  $\Theta_G$  is not converged do
2   sample  $N$  real samples  $\mathcal{D} \sim \mathbb{P}_d$  and  $N$  generated samples  $\mathcal{F} \sim \mathbb{P}_g$ ;
3   begin compute the discriminator loss
4   |  $L_D \leftarrow \sum_{x \in \mathcal{D}} [-\log(D(x))] + \sum_{x \in \mathcal{F}} [-\log(1 - D(x))]$ 
5   end
6    $\Theta_D \leftarrow \Theta_D - \alpha \nabla_{\Theta_D} L_D$ .
7   begin compute the generator’s loss
8   |   compute the features  $D'(\mathcal{D})$  and  $D'(\mathcal{F})$ .
9   |   compute  $L_G$  in Equation 10; for  $\sqrt{\Sigma_d^{D'} \Sigma_g^{D'}}$ , compute its value using
   |     Newton Schultz iterations in Equation 13 and its derivative by solving
   |     Equation 12.
10  end
11   $\Theta_G \leftarrow \Theta_G - \alpha \nabla_{\Theta_G} L$ .
12 end

```

---

available on Github<sup>5</sup>. We alternately train the discriminator and the generator. In each iteration, we draw samples from the real and generated distributions  $\mathbb{P}_d$  and  $\mathbb{P}_g$ , respectively. Then, we train the discriminator, for  $k$  iterations, to learn the feature space that best discriminates the real and generated samples. To update the generator, we perform the forward pass to compute the Fréchet distance in the feature space defined by  $D'$ . For the square root term  $\sqrt{\Sigma_d^{D'} \Sigma_g^{D'}}$ , we perform the forward pass using the proposed Newton-Schultz iterative algorithm and perform the backward pass by solving the Sylvester Equation, defined in Equation 12, using the Bartels-Stewart algorithm. In our implementation, we rely on automatic differentiation by keeping the computation graph of the iterative computation in memory.

The computation cost of Fréchet distance is largely dominated by the calculation of the covariance matrices and the square root term  $\sqrt{\Sigma_d^{D'} \Sigma_g^{D'}}$ . Specifically, the computation complexity using the non-iterative algorithm (using SVD) is  $O(\min(Nd^2, d^3))$ , while using the Newton Schultz algorithm, it is  $O(\min(Nd^2, Td^2))$  where  $T$  is the number of iterations. This is significantly smaller than OT’s computational cost, especially when  $N$  is large. This allows us to use a large mini-batch size to estimate the Fréchet distance, which is prohibitive for OT.

## 4 Experimental Results

In this section, we present experimental results to demonstrate the effectiveness of our proposed methods, specifically OT-GAN and Fréchet-GAN. We show both

<sup>5</sup> <https://github.com/khodoan/Frechet-GAN>

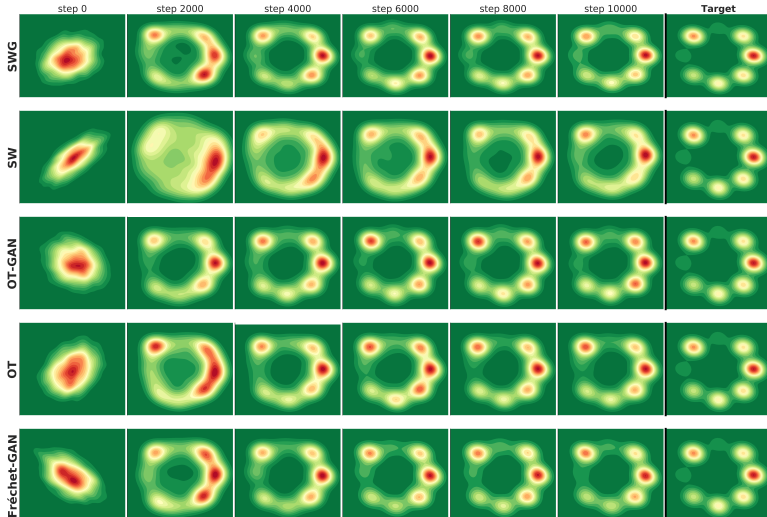


Figure 2: Dynamic results of 8-Gaussian estimation. The final column is the real distribution. SW and OT refer to minimizing Sliced Wasserstein distance and OT, respectively, without the discriminator.

the qualitative and quantitative results on the image generation task on four different popular datasets: **MNIST** [18], **CIFAR-10** [17], **CELEB-A** [19], and **LSUN-Bedroom** [25].

We compared OT-GAN and Fréchet-GAN with the following models: WGAN [21], WGAN-GP [12], SWG [8], Max-SWG [7]. For all the methods, including ours, we use the DCGAN architecture. The use of the same network architecture allows us to objectively evaluate the capabilities of methods. Wherever possible, we use the same hyperparameter setting of the baselines as provided in the original papers. In other cases, we perform model selections based on FID, and report the results from the models’ best configurations. FID is evaluated on 50,000 generated images and 50,000 real images. The best models are trained for 100 epochs on MNIST and CIFAR-10, 50 epochs on CELEB-A and 20 epochs on LSUN-Bedroom.

#### 4.1 Performance with and without the discriminator

In this section, we perform the experiment of generating the classic 8-Gaussian data [22], which has been previously used to study mode collapse. The generator and discriminator are two-hidden layer perceptions (MLPs) with Rectified-linear activation. Figure 2 shows the generated samples during the training process. Without the discriminator, both SW and OT (directly minimizing Sliced Wasserstein distance and OT respectively on the original data space) exhibit signs of mode-collapse. However, when the discriminator is used, all models, including Fréchet-GAN, can recover almost perfectly the original data. Furthermore, Fréchet-GAN converges to the target distribution more quickly than the other

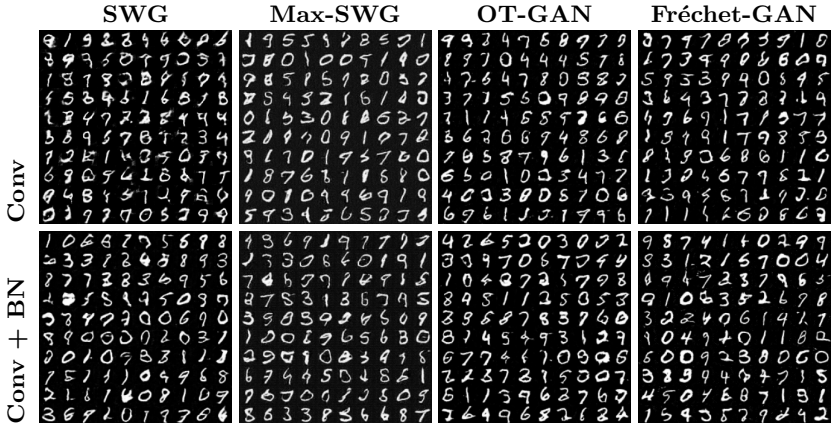


Figure 3: Generated MNIST digits with and without BN in the DCGAN Architecture.

Table 4: FID with and without BN.

		WGAN	WGAN-GP	SWG	Max-SWG	OT-GAN	Fréchet-GAN
MNIST	Conv	19.12	21.24	40.47	37.68	18.87	15.51
	Conv + BN	18.86	20.35	17.16	38.63	13.13	21.22
CIFAR-10	Conv	290.92	85.84	76.44	69.34	163.94	38.62
	Conv + BN	44.51	36.24	26.68	23.56	32.50	24.64

GANs. This experiment demonstrates the effectiveness of minimizing the distributional distances in the feature space.

Note that, for Fréchet-GAN, we simply calculate the Fréchet distance directly on the last layer of the MLP discriminator. Although this layer’s activation does not follow the multivariate Gaussian, Fréchet-GAN still works. Reasons behind such a robust behavior of Fréchet-GAN needs further investigation.

## 4.2 Stability in generating images

[21] suggests to evaluate the training stability of GANs, especially the phenomenon of mode collapse, by removing the Batch Normalization layers (BN). In this Section, we present the results for generating MNIST and CIFAR-10 images when we use the Convolution layers with and without BN.

Figure 3 shows the generated MNIST digits of two popular primal baselines, SWG and Max-SWG, as well as proposed GANs. Previously, primal GANs show significant improvement over non-Wasserstein GANs and dual-Wasserstein GANs with respect to mode collapse [8]. We observe that both OT-GAN and Fréchet-GAN can generate meaningful digits regardless of the utilization of BN.

Furthermore, without BN, Fréchet-GAN can generate digits that has a lesser degree of mode collapse, compared to the digits generated by SWG, and that are sharper, compared to Max-SWG and OT-GAN. In Table 4, we show the



Figure 5: Generated images of multi-channel datasets.

quantitative results of more compared approaches with and without BN in term of their FIDs. It is known that we can detect intra-class mode collapse through FID [4]. For both MNIST and CIFAR-10, we observe that the values of FID increase significantly, especially in CIFAR-10, without BN. However, both FID's of Fréchet-GAN and Max-SWG only slightly increase. This shows the robustness of Fréchet-GAN with respect to the model architecture; note also, the significantly smaller values of FID achieved by Fréchet-GAN (without BN).

Table 6: FIDs of the methods.

	<b>MNIST</b>	<b>CIFAR-10</b>	<b>CELEB-A</b>	<b>LSUN-Bedroom</b>
WGAN	22.44 $\pm$ 1.07	44.51 $\pm$ 0.98	24.49 $\pm$ 0.98	51.88 $\pm$ 3.21
WGAN-GP	21.40 $\pm$ 3.29	36.24 $\pm$ 0.98	22.17 $\pm$ 1.09	48.98 $\pm$ 5.25
SWG	16.89 $\pm$ 0.95	26.68 $\pm$ 0.80	10.93 $\pm$ 0.59	26.97 $\pm$ 3.42
Max-SWG	15.24 $\pm$ 1.94	<u>23.56 <math>\pm</math> 0.54</u>	10.13 $\pm$ 0.61	40.14 $\pm$ 4.51
OT-GAN	18.63 $\pm$ 0.74	32.50 $\pm$ 0.64	19.40 $\pm$ 2.98	70.49 $\pm$ 5.25
Fréchet-GAN	<u>10.51 <math>\pm</math> 2.73</u>	24.64 $\pm$ 0.54	<u>9.80 <math>\pm</math> 0.78</u>	<u>16.34 <math>\pm</math> 2.98</u>



Figure 7: High-resolution LSUN-bedroom Generated images (128x128).

### 4.3 Image Generation

In this section, we provide the results of generating images of our proposed methods and the representative baselines from both the dual and primal domains.

The generated images from different methods are presented in Figure 5. The visual quality of the images generated by OT-GAN and Fréchet-GAN is comparable to the existing GANs. Especially, Fréchet-GAN can generate images with the minimal defective artifacts. For higher-dimensional images, as shown in Figure 7, the images generated by Fréchet-GAN are comparable to those of Max-SWG. In Table 6, we present the quantitative metric, FID, of the methods. All primal-domain GANs have significant improvement over the dual-domain GANs. While OT-GAN’s FIDs are worse than those of SWG and Max-SWG, Fréchet-GAN achieves the best FIDs in MNIST, CELEB-A and LSUN-Bedroom datasets and a comparable FID to Max-SWG in CIFAR-10. This supports our claim in this paper: directly minimizing the Wasserstein distance in the feature space works for the image generative modeling task. Furthermore, Fréchet distance is heuristically shown as a more robust cost function as a proxy for estimating the Wasserstein distance for use in such image generation applications.

## 5 Conclusion

In this paper, we propose new and efficient GAN approaches which estimate the distributional distance in the low-dimensional, feature space. The feature space

is chosen from the GAN discriminator. We employ two different choices of the distributional distance, Optimal Transport and Fréchet distance, which lead to the two new GANs, OT-GAN and Fréchet-GAN, respectively. Our motivation of Fréchet-GAN is from the fact that Fréchet Inception Distance is a solid metric for evaluating the quality of the generated images and it is equivalent to the Wasserstein-2 formulation of the OT solution (but with a significant improvement in computational complexity) when the feature space distributions are multivariate Gaussians. Furthermore, we propose an efficient, differentiable algorithm to calculate the Fréchet distance. While it is previously argued that Wasserstein distance has an exponential sample complexity, it is heuristically shown that our proposed approaches to estimate the Wasserstein distance in the low-dimensional feature space overcomes such complexity of the high-dimensional space. In fact, Fréchet-GAN achieves a significant improvement in both the visual inspection of the generated images and FID, compared to the existing primal and dual GANs. The results motivate us to study other types of distributional distances in the feature space of GANs, especially in the image generation domain.

## References

1. Arjovsky, M., Bottou, L.: Towards principled methods for training generative adversarial networks. arxiv e-prints, art. arXiv preprint arXiv:1701.04862 (2017)
2. Bartels, R.H., Stewart, G.W.: Solution of the matrix equation  $ax + xb = c$  [f4]. Commun. ACM **15**(9), 820826 (Sep 1972). <https://doi.org/10.1145/361573.361582>, <https://doi.org/10.1145/361573.361582>
3. Blei, D.M., Ng, A.Y., Jordan, M.I.: Latent dirichlet allocation. Journal of machine Learning research **3**(Jan), 993–1022 (2003)
4. Borji, A.: Pros and cons of gan evaluation measures. Computer Vision and Image Understanding **179**, 41–65 (2019)
5. Burkard, R.E., Dell’Amico, M., Martello, S.: Assignment problems. Springer (2009)
6. Denman, E.D., Beavers Jr, A.N.: The matrix sign function and computations in systems. Applied mathematics and Computation **2**(1), 63–94 (1976)
7. Deshpande, I., Hu, Y.T., Sun, R., Pyrros, A., Siddiqui, N., Koyejo, S., Zhao, Z., Forsyth, D., Schwing, A.G.: Max-sliced wasserstein distance and its use for gans. In: Proceedings of the IEEE Conference on Computer Vision and Pattern Recognition. pp. 10648–10656 (2019)
8. Deshpande, I., Zhang, Z., Schwing, A.G.: Generative modeling using the sliced wasserstein distance. In: Proceedings of the IEEE conference on computer vision and pattern recognition. pp. 3483–3491 (2018)
9. Doan, K., Kimiyaie, A., Manchanda, S., Reddy, C.K.: Image hashing by minimizing independent relaxed wasserstein distance. arXiv preprint arXiv:2003.00134 (2020)
10. Genevay, A., Peyré, G., Cuturi, M.: Learning generative models with sinkhorn divergences. arXiv preprint arXiv:1706.00292 (2017)
11. Goodfellow, I., Pouget-Abadie, J., Mirza, M., Xu, B., Warde-Farley, D., Ozair, S., Courville, A., Bengio, Y.: Generative adversarial nets. In: Advances in neural information processing systems. pp. 2672–2680 (2014)
12. Gulrajani, I., Ahmed, F., Arjovsky, M., Dumoulin, V., Courville, A.C.: Improved training of wasserstein gans. In: Advances in neural information processing systems. pp. 5767–5777 (2017)

13. Heusel, M., Ramsauer, H., Unterthiner, T., Nessler, B., Hochreiter, S.: Gans trained by a two time-scale update rule converge to a local nash equilibrium. In: Advances in neural information processing systems. pp. 6626–6637 (2017)
14. Higham, N.J.: Stable iterations for the matrix square root. *Numerical Algorithms* **15**(2), 227–242 (1997)
15. Iohara, A., Ogawa, T., Tanaka, T.: Generative model based on minimizing exact empirical wasserstein distance (2018), <https://openreview.net/forum?id=BJgTZ3C5FX>
16. Ionescu, C., Vantzos, O., Sminchisescu, C.: Matrix backpropagation for deep networks with structured layers. In: Proceedings of the IEEE International Conference on Computer Vision. pp. 2965–2973 (2015)
17. Krizhevsky, A., Hinton, G., et al.: Learning multiple layers of features from tiny images (2009)
18. LeCun, Y.: The mnist database of handwritten digits. nec research institute (1998)
19. Liu, Z., Luo, P., Wang, X., Tang, X.: Deep learning face attributes in the wild. In: Proceedings of the IEEE international conference on computer vision. pp. 3730–3738 (2015)
20. Manchanda, S., Doan, D.K., Yadav, P., Keerthi, S.S.: Regression via implicit models and optimal transport cost minimization. arXiv preprint arXiv:2003.01296 (2020)
21. Martin Arjovsky, S., Bottou, L.: Wasserstein generative adversarial networks. In: Proceedings of the 34 th International Conference on Machine Learning, Sydney, Australia (2017)
22. Metz, L., Poole, B., Pfau, D., Sohl-Dickstein, J.: Unrolled generative adversarial networks. arXiv preprint arXiv:1611.02163 (2016)
23. Miyato, T., Kataoka, T., Koyama, M., Yoshida, Y.: Spectral normalization for generative adversarial networks. arXiv preprint arXiv:1802.05957 (2018)
24. Salakhutdinov, R., Mnih, A., Hinton, G.: Restricted boltzmann machines for collaborative filtering. In: Proceedings of the 24th international conference on Machine learning. pp. 791–798 (2007)
25. Yu, F., Seff, A., Zhang, Y., Song, S., Funkhouser, T., Xiao, J.: Lsun: Construction of a large-scale image dataset using deep learning with humans in the loop. arXiv preprint arXiv:1506.03365 (2015)